A systematic analysis of chemical mechanisms for ethylene oxidation and PAH formation

A systematic analysis of chemical mechanisms for ethylene oxidation and PAH formation

Yiqing Wang[a], Wang Han[b,*], Thorsten Zirwes[c], Antonio Attili[d], Liming Cai[e], Henning Bockhorn[c], Lijun Yang[b], Zheng Chen[a]

[a]*SKLTCS, CAPT, BIC-ESAT, College of Engineering, Peking University, Beijing 100871, China*
[b]*School of Astronautics, Beihang University, Beijing 100191, China*
[c]*Engler-Bunte-Institute, Karlsruhe Institute of Technology, Karlsruhe 76131, Germany*
[d]*School of Engineering, The University of Edinburgh, Edinburgh, Scotland EH8 3JL, UK*
[e]*School of Automotive Studies, Tongji University, Shanghai 201804, China*

Abstract

Accurate prediction of soot formation and evolution remains a formidable challenge due to the complex interaction between gas-phase composition and solid-phase particles. Recent studies have shown that the choice of gas-phase mechanisms is of primary importance in affecting predictability. In this work, a systematic analysis of ethylene (C_2H_4) combustion mechanisms denoted as KAUST, Stanford, Aachen, Polimi, ABF, DLR/UT, Naples, Caltech, and SJTU, which have been widely used in the soot community, is performed to investigate their differences in fundamental chemistry, polycyclic aromatic hydrocarbon (PAH) chemistry, and soot prediction. It is found that the nine mechanisms exhibit large differences even in predicting canonical combustion properties (e.g., ignition delay time, laminar flame speed, and extinction strain rate), indicating significant variations in the fundamental chemistry. This is due to the fact that although most mechanisms share very similar dominant fuel-oxidation reactions, there are notable differences in the rate coefficients of sensitive reactions used in these mechanisms. Owing to the uncertainties in the fundamental chemistry, the predictions of C_2H_2 from the nine mechanisms show significant differences, which contributes to the differences in soot precursor prediction, in conjunction with the difference in benzene (A1) formation pathways demonstrated by the element flux analysis of the C atom. Furthermore, it is found that PAHs containing two rings play a dominant role in soot formation for most mechanisms. Moreover, it is observed that while Caltech and

SJTU significantly under estimate soot formation, they reasonably reproduce its sensitivity to strain rate. These results indicate that despite substantial advances in the development of C_2H_4 oxidation and PAH formation chemistry, the various existing mechanisms lead to significant differences in predicting soot concentrations which can be traced back to considerable differences in both fundamental chemistry and PAH chemistry. This suggests that the fundamental chemistry should be calibrated or improved before further development of PAH chemistry and soot models.

Keywords: Ethylene mechanism; Oxidation; PAH formation; Soot; Uncertainty

---

Contents

*Corresponding author

Email address: drwanghan@buaa.edu.cn (Wang Han)

1. Introduction

As an undesirable by-product of combustion and hazardous pollutant, soot has adverse effects on human health and is suspected to play a key role in climate change. Therefore, control and reduction of soot emission have been one of the main concerns in the development of low-emission propulsion and power systems. However, reliable simulations of sooting flames remain a scientific challenge and the combustion community dedicates significant efforts on this topic [1, 2]. This is due to the complexity of physico-chemical processes involved in soot formation and evolution, including soot precursor reactions, nucleation, coagulation, condensation, heterogeneous surface reactions and the underlying aerosol/flow dynamics [3–6]. All these make soot modeling one of the hardest problems in combustion research [1–5, 7].

Soot models have three main components [7]: Model-I for aerosol/flow dynamics, Model-II for physico-chemical processes of particle formation, growth and oxidation, and Model-III for fuel oxidation and soot precursor (i.e., polycyclic aromatic hydrocarbons - PAHs) formation/growth. The focus of this work is the latter aspect, Model III, with special attention on ethylene (C_2H_4) oxidation and PAH formation chemistry, given the importance of the C_2H_4 fuel in understanding soot formation and evolution as well as validating soot models. While tremendous progress has been made towards the development of C_2H_4 oxidation and PAH formation chemistry [8–31], recent studies [32–36] have concluded that the choice of chemical mechanisms (i.e., Model-III) is of primary importance in affecting predictability.

Despite the significance of Model-III in predicting soot concentrations, there are only few investigations attempting to reveal the sensitivity of the prediction to the choice of Model-III. Chong et al. [32] compared two C_2H_4 mechanisms, the KAUST skeletal mechanism [8, 9] and the Stanford (or NBP) mechanism [19, 20], in terms of their abilities to predict soot formation in C_2H_4 swirling flames. Similar to [9, 35] when simulating laminar sooting flames, they found that the KAUST mechanism calculates higher soot concentrations than the Stanford mechanism. This could be attributed to the inclusion of large PAH species up to coronene (A7) in the KAUST mechanism. Abdelgadir et al. [33] compared the Stanford mechanism

with the KAUST-USC Mech [31], and reported that the peak pyrene (A4) mole fraction predicted by the KAUST-USC mechanism is about 70 times higher than that by the Stanford mechanism in a coflow C_2H_4 diffusion flame at 8 atm. Kruse et al. [34] also examined two C_2H_4 mechanisms: the Aachen mechanism [22] and the Polimi mechanism [23], in terms of their performance in predicting the sensitivity of soot formation to strain rate in counterflow diffusion flames of C_2H_4 and gasoline surrogate components. They reported that in some cases the Aachen mechanism appeared to be more accurate than the Polimi mechanism.

Table 1: Mechanisms for C_2H_4 oxidation and PAH formation/growth, in which both Caltech and Aachen mechanisms were developed based on Stanford (or NBP) mechanism [19, 20]. More details about H_2/CO and C_3-C_5 sub-mechanisms used in the nine mechanisms are provided in corresponding references.

Mech	Species#/Reactions #	Fundamental chemistry	Aromatic chemistry	Reference
KAUST	99/625	AramcoMech 1.3 [29]	C_6H_6- $C_{24}H_{12}$ or A1-A7	[9]
ABF	101/544	GRI-Mech 1.2 [37]	C_6H_6-$C_{16}H_{10}$ or A1-A4	[11]
DLR/UT	112/881	LeedsMech [38]	C_6H_6- $C_{20}H_{12}$ or A1-A5	[13]
Naples	117/407	GRI-Mech 3.0 [39]	C_6H_6-$C_{16}H_{10}$ or A1-A4	[17, 18]
Stanford	158/1049	Optimized GRI-Mech 3.0 [39–41]	C_6H_6-$C_{18}H_{10}$ or A1-A4R5	[20]
Polimi	170/5465	POLIMI [23]	C_6H_6-$C_{16}H_{10}$ or A1-A4	[24]
Caltech	174/1896	Optimized GRI-Mech 3.0 [39–41]	C_6H_6-$C_{18}H_{10}$ or A1-A4R5	[21]
SJTU	182/1167	SJTU [25, 26, 28]	C_6H_6- $C_{16}H_{10}$ or A1-A4R5	[27]
Aachen	339/1693	Optimized GRI-Mech 3.0 [39–41]	C_6H_6-$C_{18}H_{10}$ or A1-A4R5	[22]

It should be noted that the focus of the above investigations [32–34] is mainly placed on the impact of the choice of Model-III on predicting soot concentrations in sooting flames. This may lead to an insufficient understanding about the differences in PAH chemistry due to notable removal of PAHs in soot formation/growth processes. Moreover, only two mechanisms are investigated in the above studies [32–34] with special attention on the difference in PAH chemistry. Therefore, it is now indispensable to question what differences in PAH chemistry exist among the most widely used C_2H_4 mechanisms in the soot community. In addition to the differences in the PAH chemistry, investigations on the differences in fundamental (i.e., C_0-C_2) chemistry are still lacking, while the C_0-C_2 chemistry can play a substantial role in mechanism performance and subsequent PAH formation.

To address the above gaps, nine C_2H_4 combustion mechanisms which have been widely used in the soot community will be investigated in this work in terms of their differences in fundamental chemistry, PAH chemistry, and prediction of soot concentrations. The nine mechanisms are summarized in Table 1 and denoted as KAUST, Stanford, Aachen, Polimi,

ABF, DLR/UT, Naples, Caltech, and SJTU. The Caltech mechanism is downloaded from its official website[42], while the Stanford and Naples mechanism files are obtained from the supplementary materials of corresponding papers [17, 18, 20]. For Aachen, ABF, DLR/UT, KAUST, Polimi, and SJTU mechanisms, they are directly sent by their developers, respectively. It is seen that the nine mechanisms were developed using different fundamental and PAH chemistry. The ABF mechanism by Appel et al. [11] is a detailed mechanism which was validated against the profiles of major and minor species, aromatics, and soot yielding in premixed flames of ethane, ethylene and acetylene with various C/O ratios (0.6-1.3) at wide pressure conditions (0.12-10 bar). The Stanford mechanism [20] was proposed on the basis of the detailed mechanism by Blanquart et al. [19] which has been developed for the oxidation of a wide range of hydrocarbon fuels ranging from methane up to large hydrocarbon components (e.g. C_7H_{16} and C_8H_{18}) and has incorporated the sub-mechanism for the formation of larger PAH molecules up to cyclo[cd]pyrene. In the Stanford mechanism [20], the base mechanism in [19] was extended to include the combustion of some other aromatics, namely ethylbenzene, styrene, 1-methylnaphthalene, and m-xylene. It has been extensively validated against IDTs and LFSs over a wide range of temperatures and pressures as well as the soot precursor formation in premixed flat flames of n-heptane and iso-octane and counterflow diffusion flames of acetylene and n-heptane. Based on the Stanford mechanism, Cai and Pitsch [22] updated the modules for Primary Reference Fuel mixtures (i.e., n-heptane and iso-octane) and ethanol in the Aachen mechanism, while Blanquart et al. [21] further made some modifications to improve the predictive capabilities of the Stanford mechanism in the development of the Caltech mechanism. The SJTU mechanism by Yuan et al. [25–28] is a detailed mechanism with special attention on the pyrolysis and oxidation toluene and o-xylene and has been validated and improved for the laminar premixed ethylene flames at elevated pressures. The DLR/UT mechanism by Dworkin et al. [13] is a gradual upgrade of the mechanism proposed by Slavinskaya et al. [12] which was developed to predict the formation/growth of PAH up to five aromatic rings in methane and ethylene-fueled flame. The KAUST mechanism by Selvaraj et al. [9] was built from the detailed mechanism AramcoMech 1.3 [29] for the fuels up to C2 and chemical pathways for PAH up to A7 [8], which has been

validated against the laminar non-premixed and premixed ethylene flames at atmospheric pressure. The Polimi mechanism by Ranzi and coworkers [23, 24] is hierarchically organized and is based on the detailed mechanism for the C1-C4 chemistry which has been validated against a large amount of experimental data [23]. The Naples mechanism by D'Anna et al. [17, 18] was developed on the basis of GRI Mech 3.0 [39] for C1-C2 species and has been validated over a range of different operating conditions in rich premixed laminar ethylene flames. While these mechanisms date back to very different years, they are still widely used in the soot community nowadays. For more detailed information about the fuel types and parameter sets that these mechanisms aim to predict, please refer to the corresponding references listed in Table 1. Given that the nine mechanisms are widely used for studying soot formation in ethylene flames in the literature [8–31], the analysis and comparison of these mechanisms are of importance.

It is noted that the PAH chemistry is typically developed with the specific fundamental chemistry they were designed for. In this context, it is difficult to completely decouple PAH and fundamental chemistry because different mechanisms have different species for instance, and that the performance of a PAH subset on different core mechanism might be worse, etc. Recently, some efforts have been made [43] to the integration of kinetic subsets from different research groups so that a detailed chemical kinetic model which consists of separate and independent fundamental (core) chemistry and PAH chemistry can be obtained.

With this background, the objective of this work is threefold:

1. To investigate the fundamental chemistry of the nine mechanisms through analysis of three performance indicators, i.e., laminar flame speed, ignition delay time, and extinction strain rate, combined with a sensitivity analysis to identify underlying differences in the fundamental chemistry;
2. To examine the predictabilities of the nine mechanisms to large hydrocarbon species, combined with an element flux analysis of the carbon (C) atom to identify differences in the pathways from fuel to benzene (A1);
3. To assess the sensitivity of soot prediction to the choice of mechanisms and the contributions of PAHs.

To the authors' knowledge, this study is the first attempt to perform a systematic analysis of chemical mechanisms for ethylene oxidation and PAH formation. In order to achieve the above three objectives, the differences among the nine mechanisms are examined at the three levels (see Fig. 1): fundamental chemistry, PAH chemistry, and soot predictions. It is noted that the intention of this work is to investigate the differences of chemical mechanisms for C_2H_4 oxidation and PAH formation as well as to identify underlying reasons leading to the differences, rather than to assess which mechanisms are more accurate than others.

The paper is structured as follows. In the next section, the descriptions of numerical details and experimental data are presented, followed by the description of sensitivity analysis and element flux analysis. The results and discussion are presented in Section 3, in which the fundamental chemistry of the nine mechanisms is first investigated in Section 3.1; the predictabilities of the nine mechanisms to large hydrocarbon species are examined and the differences in the pathways from fuel to benzene (A1) are identified in Section 3.2; and then, the sensitivity of soot prediction to the choice of mechanisms is quantified in Section 3.3. Finally, the conclusions are summarized in Section 4.

2. Methodology

2.1. Numerical details and experimental data

To reveal whether the nine mechanisms exhibit differences in the fundamental chemistry, ignition delay time (**IDT**), laminar flame speed (**LFS**), and extinction strain rate (**ESR**) are employed as performance indicators (see Fig. 1). The IDTs are calculated in homogeneous reactors at the pressure of $P = 1.1\,\text{atm}$ and equivalence ratio of $\phi = 1$ and 2. The LFSs are obtained by simulating 1D freely-propagating premixed C_2H_4/air flames at $0.5 < \phi < 3.0$ and room temperature and pressure conditions. The ESRs are calculated by counterflow diffusion flames at $P = 1\,\text{atm}$ with $12.2\%C_2H_4$+$87.8\%N_2$ in volume at the fuel side and air at the oxidizer side. These quantities are calculated using Cantera [44] with the nine mechanisms. The time and spatial resolutions are examined to ensure the convergence of solutions. The conditions used to obtain the IDTs, LFSs, and ESRs are chosen to match

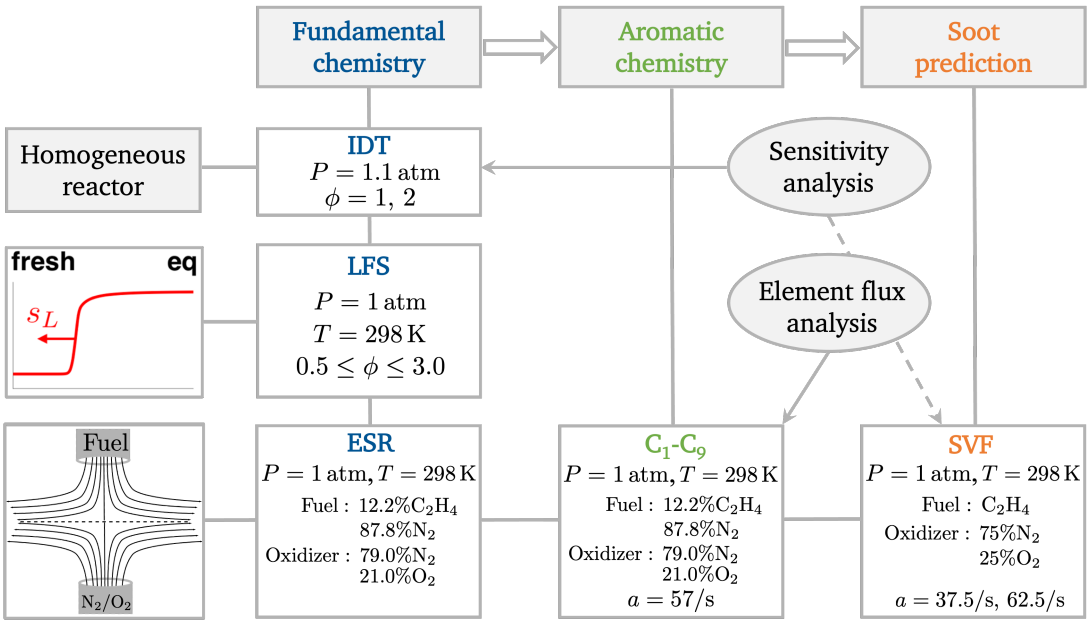

Figure 1: Scheme of numerical configurations and targets for performing the systematic analysis of chemical mechanisms for ethylene's fundamental chemistry and aromatic chemistry, in which the targets IDT, LFS, ESR, and SVF represent ignition delay time, laminar flame speed, extinction strain rate, and soot volume fraction, respectively. The details of sensitivity analysis and element flux analysis are provided in Section 2.2.

with the corresponding IDT [30], LFS [45], and counterflow [46] experiments in the literature. The readers who are interested in the uncertainty of experimental date can refer to [30, 45, 46]. It is noted that in this work the experimental data sets are selected based on the consideration that the thermodynamics condition and mixture composition should be as normal as possible, such that they are well within the range of application of each mechanism. On the other hand, the intention of this work is not to give a ranking on these mechanisms, the experimental data are used here only for reference and hence only sufficient experimental data are considered in this work.

To achieve the second objective in terms of the differences of PAH chemistry in the nine mechanisms, the Yale soot-free counterflow experiment [46], in which the distributions of C_1-C_9 species were measured, is simulated using Cantera at the same conditions as the above ESR calculations but with a fixed global strain rate of $a = 57$/s, as shown in Fig. 1. Here the global strain rate is defined as $a = (U_F + U_{Ox})/L$, based on the nozzle distance L and fuel (U_F) and oxidizer (U_{Ox}) inlet velocities. The non-sooting flame is considered to

avoid the notable removal of PAHs in soot formation/growth processes so as to reach better understanding about the differences in PAH chemistry.

In order to examine the impact of the choice of mechanisms on the sensitivity of soot concentrations to PAH chemistry and strain rate, two sooting counterflow diffusion flames [47] at $a = 37.5/\mathrm{s}$ and $a = 62.5/\mathrm{s}$ with pure C_2H_4 and $25\%O_2/75\%N_2$ in volume at the fuel and oxidizer sides, respectively, are simulated using an OpenFOAM-based in-house solver [48]. A state-of-the-art statistical soot model, the Hybrid Method of Moments (HMOM) [49–54], considering PAH based nucleation and condensation, coagulation, surface growth, oxidation, and fragmentation processes has been implemented into this solver. The HMOM method is used for its numerically efficiency and robustness as well as its ability to account for the bimodality of the soot size distribution. It is noted that the overall analysis is limited by the choice of a single soot model, as different parts of the gas phase chemistry (i.e., different PAHs coupled with the soot mechanism) will affect the results obtained.

The difficulty faced with examining the impact of chemical mechanisms on soot prediction is that any soot model has its own peculiarity to be considered in this kind of juxtaposition often leading to misinterpretation and misquotation. The compromise is to perform this comparison defining clear interfaces between the different components of the overall model: i) combustion chemistry, ii) particle formation and growth, and iii) soot prediction. Therefore, the comparison does not refer to different soot models, but takes just one soot model plugged on the gas phase interface provided by different reaction mechanisms. Any soot model offers numerous features beyond those ones covered by the HMOM model. For example, applying the complete ABF-model (or others) certainly would have brought about different results. However, the complete ABF-soot model (or other soot models) is not subject of the comparison.

Furthermore, the conversion and coupling between the solid-phase and gas-phase are carefully addressed, and the radiation from the gas-phase and solid-phase is described by the optically thin model. More details about the two-phase coupling and radiation modeling are provided in our previous work [55, 56]. It is noted that the same model parameters (e.g., sticking coefficients, collision frequency, and surface reaction coefficients) are used when

coupling HMOM with the nine mechanisms for a fair comparison. Nevertheless, the difference in the soot precursors (i.e. PAHs) considered in the nine mechanisms (see Table 1) can lead to different dimer concentrations required for nucleation and condensation. More details about the rate of PAH dimerization are provided in Supplement A.

2.2. Sensitivity analysis and element flux analysis

Brute-force sensitivity analysis is a useful approach to determine rate limiting reactions. In this work, the sensitivity analysis is conducted for IDT to identify key reactions in fuel oxidation with the normalized sensitivity coefficients given by $S_i = \partial \ln \tau / \partial \ln k_i$, measuring the sensitivity of IDT (τ) to the change of the rate coefficient (k_i) of reaction i. Although the sensitivity analysis for IDT and LFS can be readily applied, only the sensitivity analysis for IDT is presented since they provide very similar results (which would be shown later).

To identify the differences of the nine mechanisms in the pathway from fuel to A1, the element flux analysis [57] is performed for the Yale counterflow flame. The species A1 is chosen here because it serves as an important bridge linking the fuel oxidation and PAH formation/growth. The flux analysis can provide a metric to quantify species activity during element (e.g. C) transformation and gain insights into the privileged reaction pathways. The instantaneous element flux of the C atom from species j to species k through reaction i, $C^i_{j\to k}$, and the total element flux, $C_{j\to k}$, are defined as

$$C^i_{j\to k} = \dot{q}_i \frac{n_{C,j} n_{C,k}}{N^i_C}, \text{ and } C_{j\to k} = \sum_i C^i_{j\to k}, \tag{1}$$

where q_i is the net production rate of reaction i, $n_{C,j}$, $n_{C,k}$ the number of C atoms in species j and k, respectively, and N^i_C the total number of C atoms in reaction i. To obtain global information, a space-integrated flux is proposed as $\overline{C}_{j\to k} = \int_0^L C_{j\to k}(x)dx$ where x is the spatial coordinate.

The conventional flux analysis is based on outflow flux. Specifically, the importance of reaction pathway $A \to B$ is characterized by the ratio between the outflow flux from species A to species B and the total outflow flux from species A. Starting from fuel species,

e.g. C_2H_4, and tracking the outflow flux along with important pathways, the dominant reaction pathways from fuel to products are identified. However, this methodology can not be applied to identify the reaction pathways from fuel to A1 as the production of A1 is very small compared to major products, e.g. CO_2 and CO. For this reason, a backward flux analysis which is based on the inflow flux is adopted in this work. Note that normalizing each inflow flux of species B by the total inflow flux to species B can qualitatively evaluate the contributions of each parental species of species B to its carbon mass. Therefore, starting from A1 and tracing back the main source of C atom, it will finally end at fuel, C_2H_4, such that the main reaction pathways from C_2H_4 to A1 can be identified. In this context, the element flux pathway of C atom used in this work, $A \xrightarrow{n} B$, represents that the contribution of the species A to the carbon mass of the species B accounts for $n \times 100\%$.

It is straightforward that the analysis of PAH chemistry and soot prediction is directly related to soot formation. As for the fundamental chemistry, it is generally accepted that it could influence soot formation through the chemical kinetic perspective, e.g., the production of some important small species and some large hydrocarbon species.

3. Results and discussion

In this section, a systematic analysis of chemical mechanisms for ethylene oxidation and PAH formation is performed. First, the fundamental chemistry of the nine mechanisms is first investigated in Section 3.1 through analysis of three performance indicators, i.e., IDT, LFS, and ESR, combined with a sensitivity analysis to identify underlying differences in the fundamental chemistry. Then, the predictabilities of the nine mechanisms to large hydrocarbon species are examined and the differences in the pathways from fuel to A1 are identified through an element flux analysis of the carbon (C) atom in Section 3.2. Finally, the sensitivity of soot prediction to the choice of mechanisms is examined in Section 3.3.

3.1. Fundamental chemistry

Previous studies have demonstrated that IDTs, LFSs, and ESRs of C_2H_4/air mixtures are mainly determined by the fundamental chemistry [58]. Therefore, the three quantities are

chosen as performance indicators of the nine mechanisms to examine their differences in the fundamental chemistry. Figure 2 compares predicted IDTs of premixed C_2H_4/air mixtures as a function of initial temperature T_0 at $P = 1.1$ atm, and $\phi = 1$ and 2. The experimental data from [30] is included for comparison. It is noted that the numerical and shock-tube IDTs are determined at $(dT/dt)_{\max}$ and $(dP/dT)_{\max}$ [30], respectively. As depicted in Fig. 2, while a similar trend appears for all the mechanisms except for DLR/UT, significant differences in IDT predictions are observed among the nine mechanisms. Specifically, the IDTs predicted by the Naples, ABF and Aachen mechanisms are considerably longer than those predicted by the other six mechanisms at both $\phi = 1$ and 2, among which the Naples mechanism gives the highest IDT, about two orders of magnitude higher than measured data. Moreover, the IDTs predicted by the Stanford and Caltech (or KAUST and SJTU) mechanisms are very similar, slightly larger than (or close to) the experimental data. On the other hand, the lowest IDTs are predicted by the Polimi mechanism.

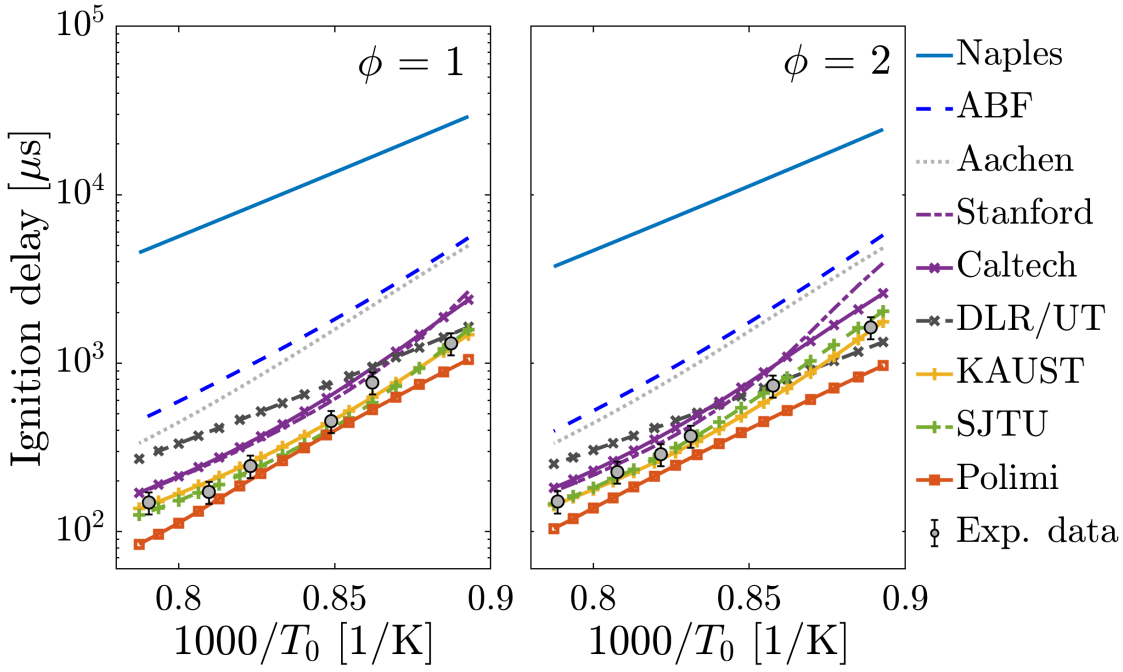

Figure 2: Ignition delay times (IDTs) of C_2H_4/air at $P = 1.1$ atm, $\phi = 1$ (left) and $\phi = 2$ (right) , in which the numerical and shock-tube IDTs are determined at $(dT/dt)_{\max}$ and $(dP/dT)_{\max}$ [30], respectively. The maximum values of T_0 are 1265 K and 1268 K for $\phi = 1.0$ and 2.0, respectively. (For interpretation of the references to color in this figure legend, the reader is referred to the web version of this article.)

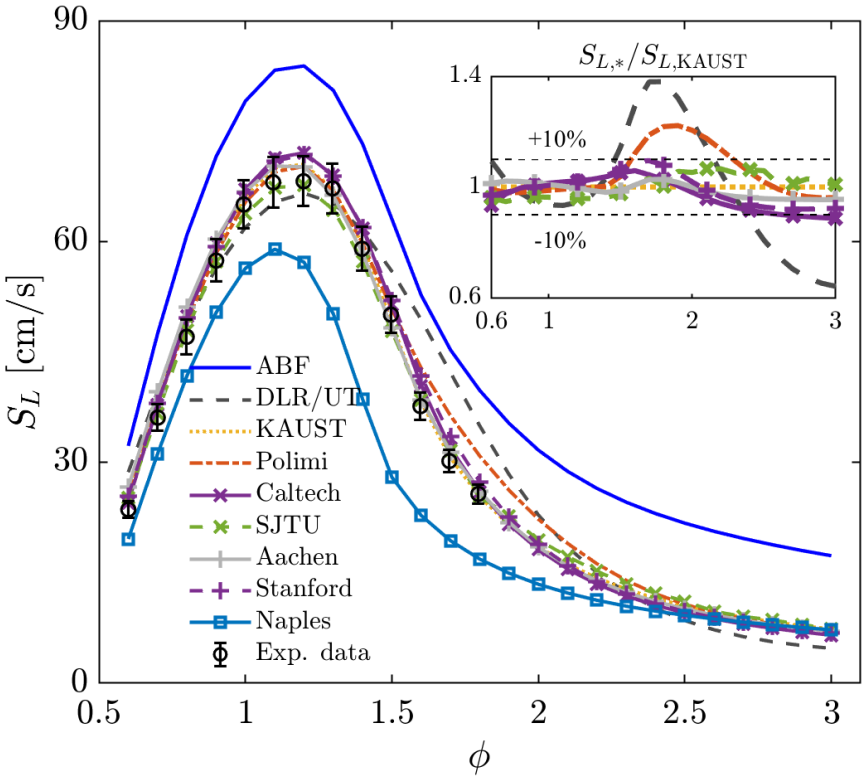

Figure 3: Laminar flame speeds (LFSs) of C_2H_4/air at room temperature and pressure. The relative comparison is shown in the inserted figure. Experimental data from [45]. (For interpretation of the references to color in this figure legend, the reader is referred to the web version of this article.)

To further investigate the fundamental chemistry, the LFSs of premixed C_2H_4/air predicted by these mechanisms are shown in Fig. 3 at normal temperature and pressure conditions with $\phi = 0.5$ to 3.0. The experimental data from [45] is also included as a reference. It is seen that the LFSs predicted by the KAUST, Caltech, SJTU, Aachen and Stanford mechanisms are in good agreement within a 10% relative error when scaled by the LFS predicted by KAUST. This is indicated in the inserted figure in Fig. 3. The predicted LFSs by the DLR/UT and Polimi mechanisms show deviations from the LFSs predicted by the above five mechanisms at rich conditions ($\phi > 1.5$). Furthermore, the predicted LFSs by the ABF and Naples mechanisms are obviously higher and lower, respectively, than those by the other seven mechanisms. It is noted that the experimental data measured by several groups at atmospheric pressure is also considered for comparison in Supplementary Material

B. It is found that the uncertainties in chemical mechanisms are much more remarkable than the uncertainties in the experimental data. Given that the objective of this study is to reveal the uncertainties in chemical mechanisms, only one set of recent experimental data measured by Huo et al. [45] is plotted for clarity.

Besides the IDT and LFS, ESR is also employed to understand the fundamental chemical reactions of the nine mechanisms. For this purpose, the variations of maximum flame temperature ($T_{\max}$) with strain rates in the counterflow diffusion flame simulated using the nine mechanisms are shown in Fig. 4. The ESRs predicted by these mechanisms are listed in the table inserted in Fig. 4. Figure 4 shows different responses of $T_{\max}$ to strain rate for these mechanisms with the highest or lowest value of $T_{\max}$ from the Polimi or DLR/UT mechanisms. Moreover, a large scatter in the ESRs is observed with a relative difference by 44% between the lowest ESR (1375/s from SJTU) and the highest ESR (1977/s from ABF).

The above analysis of IDTs, LFSs, and ESRs clearly demonstrates significant differences in the fundamental chemical reactions of the nine mechanisms. To identify key fuel-oxidation reactions that are responsible for these differences, the brute-force sensitivity analysis for IDT at $\phi = 2$ is conducted. The sensitivity coefficients for the three most positive and negative sensitive reactions in each mechanism are shown in Fig. 5, in which a total of six reactions included in most mechanisms are selected and denoted as R1-R6 here (Note that a more detailed description about the sensitivity analysis results considering five most promoting/inhibiting reactions can be found in Supplement C). It is found that reactions R1: $H+O_2=O+OH$ and R2: $C_2H_3+O_2=CH_2CHO+O$ are the most important promoting reactions in all of the mechanisms except for Naples and DLR/UT. Moreover, R3: $C_2H_5+O_2=C_2H_4+HO_2$, R4: $C_2H_3+O_2=CH_2O+HCO$, R5: $C_2H_4+O=CH_3+HCO$ and R6: $C_2H_4+H(+M)=C_2H_5(+M)$ are found to be top five inhibiting reactions in all of the mechanisms except for Naples and DLR/UT. It is noted that the sensitivity analysis of LFS is also performed and similar results can be observed (see Supplement C). Based on the above observation, it can be concluded that the dominant fuel-oxidation reactions in the Naples and DLR/UT mechanisms are very different from the other seven mechanisms. This might be one of the reasons why Naples predicts much longer IDT than the other mechanisms and

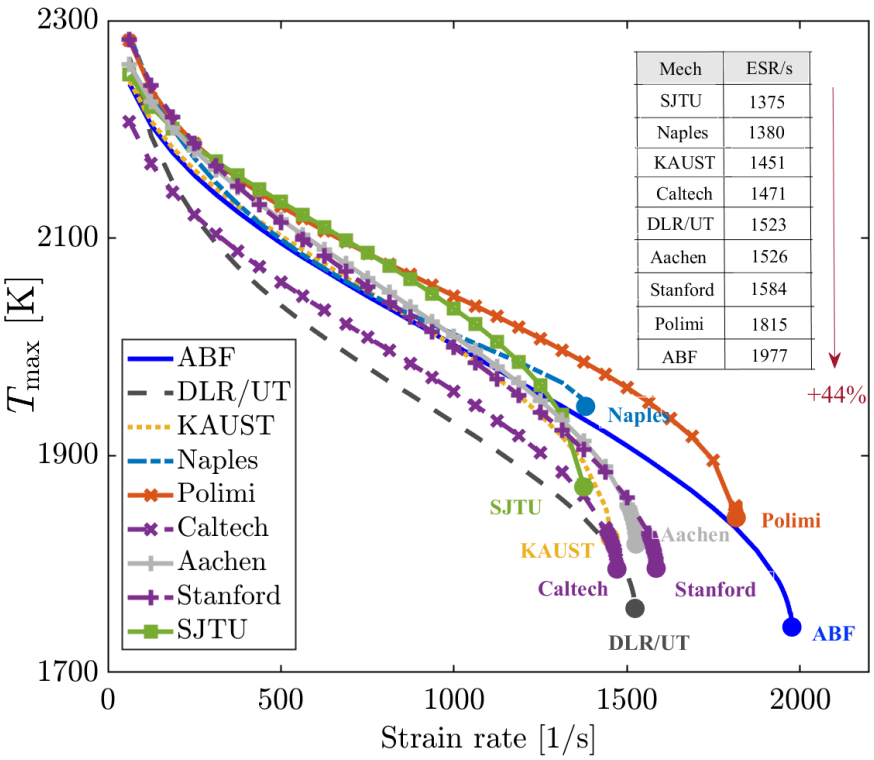

Figure 4: Response of maximum temperature to strain rate in counterflow diffusion flames with 12.2%C_2H_4+87.8%N_2 in volume at the fuel side and air at the oxidizer at $P = 1$ atm. The extinction strain rates (ESRs) are marked by filled circles. (For interpretation of the references to color in this figure legend, the reader is referred to the web version of this article.)

DLR/UT predicts a remarkably different trend of IDT as shown in Fig. 2. While the other seven mechanisms share very similar ignition driving reactions, their predictions of IDTs are still rather scattered. This could be attributed to diverse values of reaction rate coefficients used in these mechanisms. Figure 6 plots the rate coefficients of two important reactions, R2 and R4, as a function of temperature. Large discrepancies among the nine mechanisms are observed not only in the values but also in the temperature dependency of the rate coefficients, although the coefficients from the ABF, Stanford and Aachen mechanisms collapse into one curve. Furthermore, the rate coefficients of R2 from KAUST, Caltech, SJTU and Polimi exhibit different trends and are significantly lower than those from ABF, Stanford, and Aachen. For R4, Caltech and SJTU yield a similar trend but they still differ from KAUST and Polimi at $T < 1000$ K. Note that the Caltech mechanism is based on the

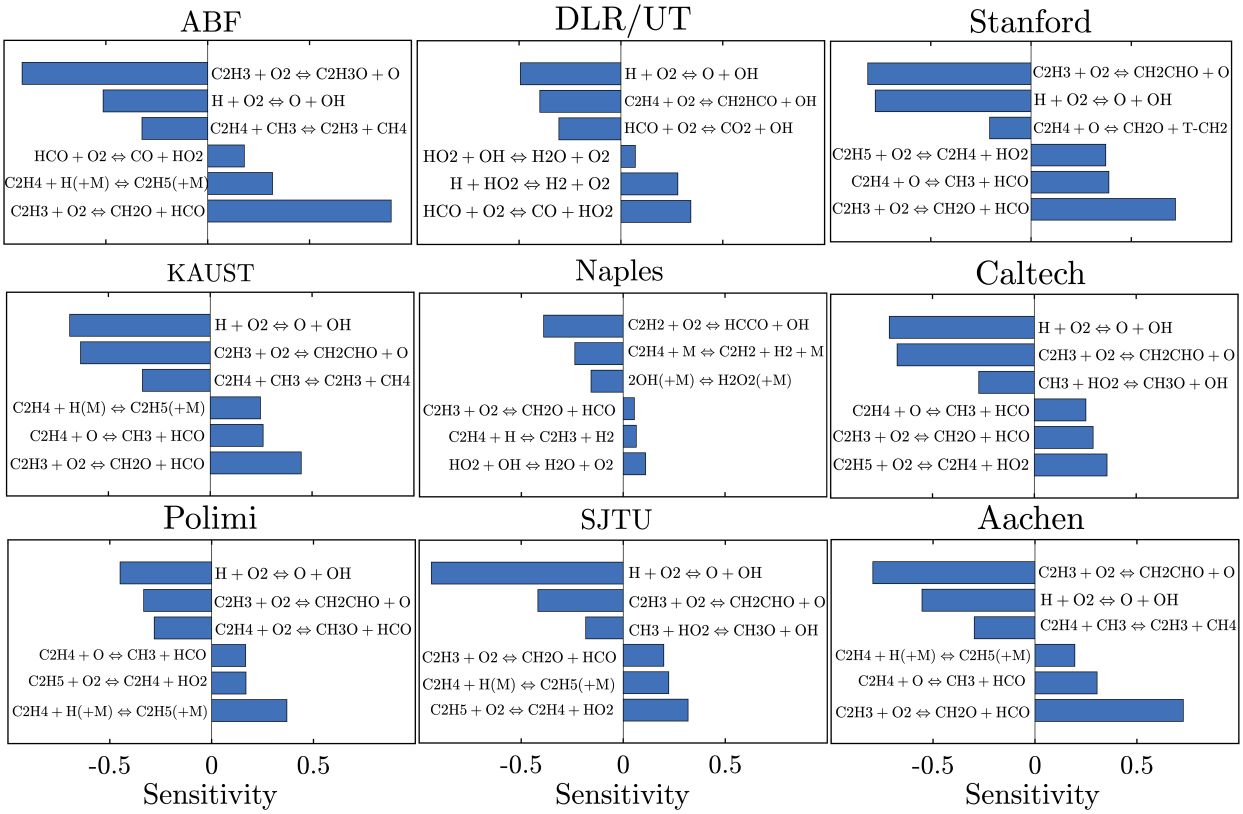

Figure 5: Sensitivity of IDT for fuel-rich ($\phi = 2$) C_2H_4/air mixture at P =1.1 atm and T =1200 K.

Stanford mechanism, whereas the above results show a discrepancy in their fundamental chemistry models. Besides, Fig. 7 shows the differences in rate coefficients of R1: H + O_2 = OH + H and C_2H_4 + CH_3 = C_2H_3 + CH_4 between Aachen and Stanford. A considerable deviation is observed. Figures 6 and 7 clearly demonstrate that although the fundamental chemistry of Stanford, Caltech and Aachen is based on the same optimized GRI-Mech 3.0, there are still some differences in their rate coefficients.

The results presented in this section show that the nine mechanisms exhibit different performance in predicting canonical combustion properties, indicating the uncertainties in the fundamental chemical reactions of the nine mechanisms, which can affect subsequent PAH formation and growth. It is noted that the above analyses are limited to the C_2H_4/air mixtures at normal temperature and pressure conditions. The comparisons for IDTs and LFSs of C_2H_4/air and C_2H_2/air mixtures at wide thermodynamic conditions are presented in Supplementary Material B. Significant deviations among the numerical predictions by

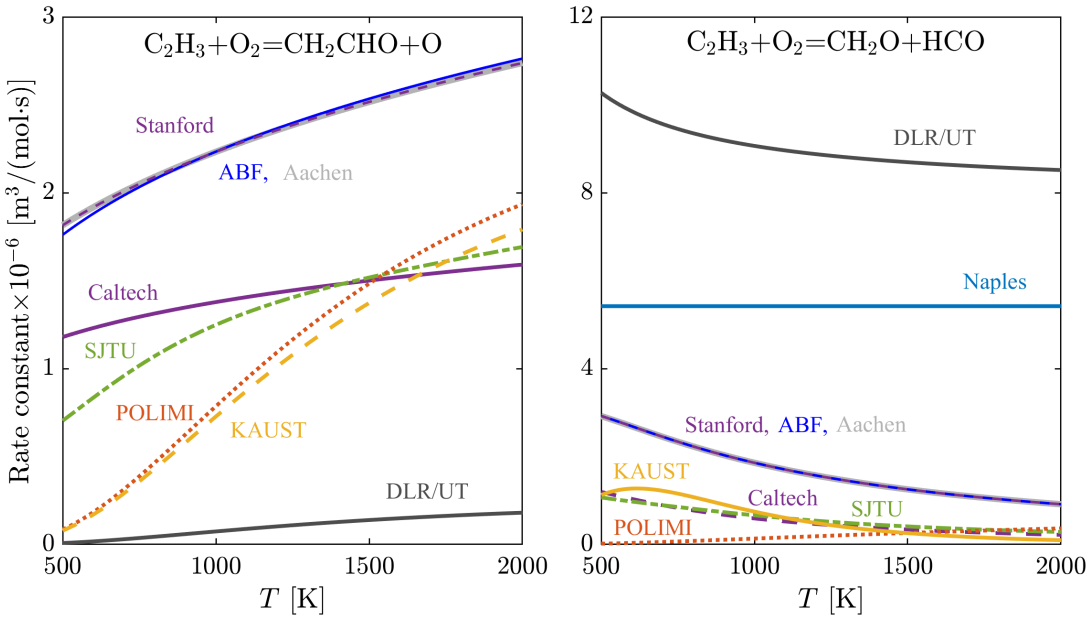

Figure 6: Rate coefficients of R2: $C_2H_3 + O_2 = CH_2CHO + O$ (left) and R4: $C_2H_3 + O_2 = CH_2O + HCO$ (right). (For interpretation of the references to color in this figure legend, the reader is referred to the web version of this article.)

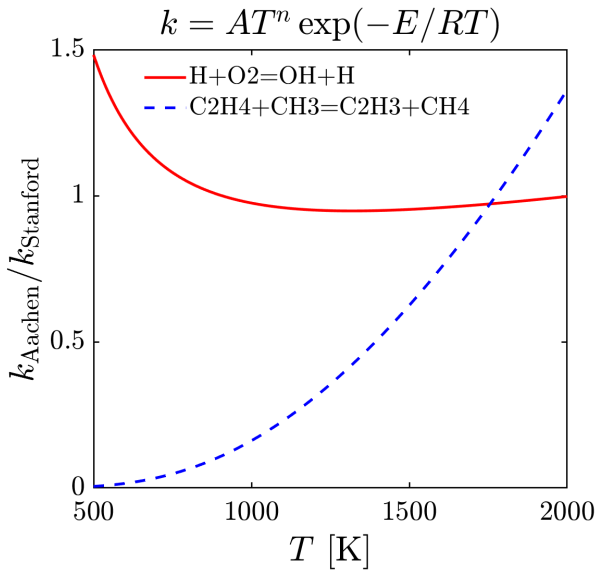

Figure 7: Comparison of rate coefficients between Aachen and Stanford for R1: $H + O_2 = OH + H$ and $C_2H_4 + CH_3 = C_2H_3 + CH_4$.

different chemical mechanisms are also observed. Moreover, the scattering patterns in the predictions for LFSs and IDTs of C_2H_4/air mixtures at elevated temperature and pressures

are similar to those at normal temperature and pressure conditions. In this sense, the differences in the performance of the nine chemical mechanisms at elevated temperature and pressure conditions are also largely attributed to uncertainties in the sensitive reactions and their reaction rate coefficients identified in this section.

3.2. Aromatic chemistry

In this section, the soot-free C_2H_4/N_2-air counterflow diffusion flame [46] described in Section 2.1 is simulated to investigate the reaction mechanisms of aromatic species in the nine mechanisms. Figure 8 shows the distributions of measured and simulated mole fractions of some intermediate species and soot precursors. While all the mechanisms give good and according predictions of main species distributions (such as C_2H_4, CO and CO_2, see Supplement D), their predictions on intermediate species and aromatic precursors show large scattering. It is seen that the differences in the prediction of A2 or A4 among these mechanisms are significant. For peak A4 mole fraction, the highest value predicted by DLR/UT is about five orders of magnitude larger than the lowest value predicted by Aachen/Stanford. Compared to soot precursors, the differences in predicted small intermediate species are relatively moderate but still noticeable. The comparison for some important radicals, such as C_3H_3, n-C_4H_5, i-C_4H_5 and phenyl can be found in Supplement D. Significant differences in the predictions of these species by the nine mechanisms are also observed. It will be shown later in the pathway analyses for A1 and C_5H_6 formation that these species are of great importance in the formation of A1 and large aromatics, such as the combination of two C_3H_3 radicals and the reaction between C_2H_2 and n-C_4H_5/i-C_4H_5.

Furthermore, Fig. 9 plots the characteristics time scales (τ_c) for some critical species, namely CO_2, C_2H_2, A2 and A4, in mixture fraction space. Given that the combustion process is mainly controlled by slow reactions, the emphasis is placed on τ_c in the vicinity of stoichiometric mixture, where τ_c reaches its lowest value. For the major species, CO_2, τ_c obtained in the nine mechanisms are close to each other, while for intermediate species, C_2H_2, τ_c predicted by DLR/UT is much larger than the other mechanisms. For larger hydrocarbons, e.g., A2 and A4, τ_c predicted by various mechanisms span a larger range,

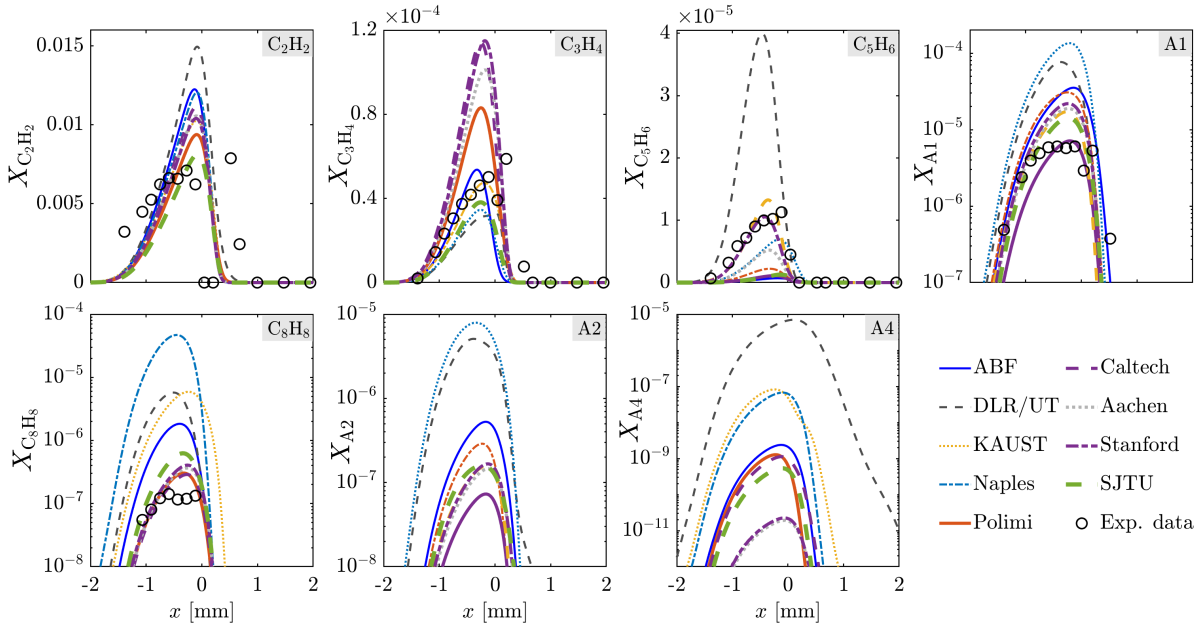

Figure 8: Mole fractions of soot precursors in the soot-free C_2H_4/N_2-air counterflow diffusion flame at $P = 1$ atm with 12.2%C_2H_4+87.8%N_2 in volume at the fuel side and air at the oxidizer side. Experimental data is taken from [46]. (For interpretation of the references to color in this figure legend, the reader is referred to the web version of this article.)

which is consistent with the results in Fig. 8.

The above results demonstrate diversity in PAH chemistry in the nine mechanisms. In order to further investigate PAH chemistry, the element flux analysis of the C atom is performed to identify the pathways from C_2H_4 to A1, as shown in Fig. 10. The species A1 is chosen here because it can serve as a connection between fuel oxidation and PAH formation/growth. It is seen from Fig. 10 that for ABF, Polimi, Stanford and Aachen mechanisms, A1 primarily originates from C_3H_3, either via the recombination of two C_3H_3 radicals (in ABF and Polimi) or via an intermediate reaction where two C_3H_3 radicals form fulvene ($C_5H_4CH_2$) which then isomerizes to A1 (in Stanford and Aachen). Note that in ABF, Stanford and Aachen, C_3H_3 is mainly produced from acetylene (C_2H_2) while in Polimi, the H-abstraction reactions from allene (a-C_3H_4) to C_3H_3 is of primary importance. For Caltech, although A1 is also dominantly produced from $C_5H_4CH_2$ similar to Aachen and Stanford, the formation pathway for $C_5H_4CH_2$ is augmented through the reaction between C_2H_2 and n-C_4H_5/i-C_4H_5. In contrast, for DLR/UT A1 is directly produced via the reaction be-

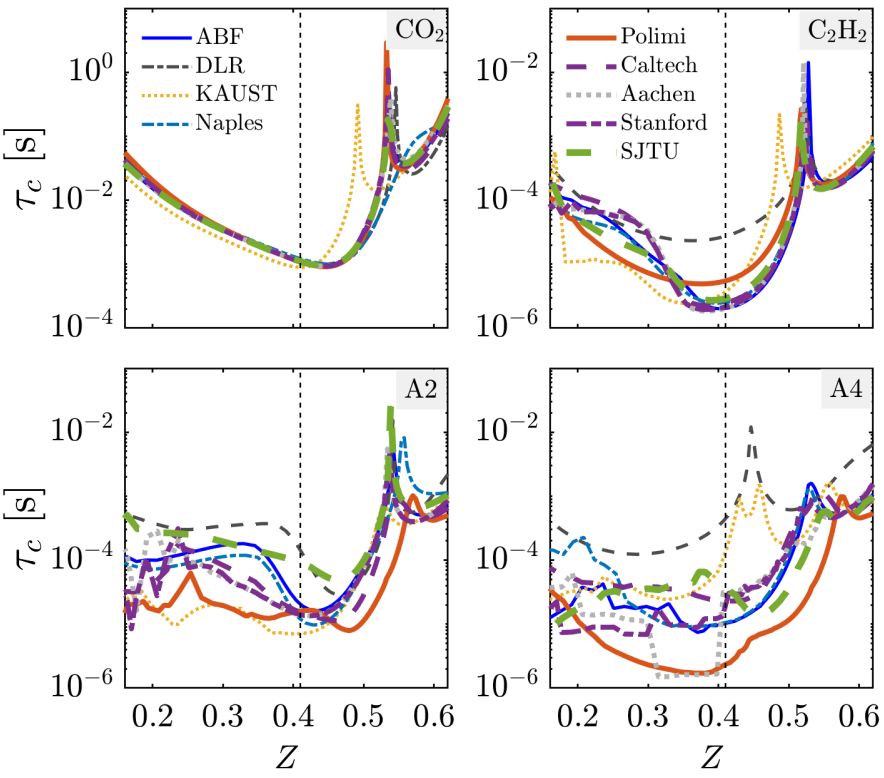

Figure 9: Characteristic time scales of critical species in the soot-free C_2H_4/N_2-air counterflow diffusion flame at $P = 1$ atm with 12.2%C_2H_4+87.8%N_2 in volume at the fuel side and air at the oxidizer side. The stoichiometric mixture fraction is indicated by a vertical dashed line. (For interpretation of the references to color in this figure legend, the reader is referred to the web version of this article.)

tween C_2H_2 and i-C_4H_5 without the involvement of $C_5H_4CH_2$. Unlike the above mentioned mechanisms, A1 is mainly formed from $C_6H_5CH_3$ through the H atom addition reaction (i.e., $C_6H_5CH_3$+H=A1+CH_3) in Naples. For KAUST, multiple A1 formation pathways are observed, in which C_3H_3, C_4H_5-2 and $C_6H_5CH_3$ contribute equally to A1 formation. On the other hand, for SJTU A1 dominantly originates from C_4H_4, C_5H_3 and C_2H_3 in descending order, which is fundamentally different from the above identified pathways. The comparison of A1 formation pathways reveals that there are substantial differences in A1 formation pathways among the nine mechanisms, especially in terms of the dominant source of small molecules.

Moreover, Fig. 10 shows the importance of the small species, i.e., C_2H_2, in the A1 formation process. Since the H-Abstraction-C_2H_2-Addition (HACA) mechanism is considered in

both PAH formation and soot surface reactions, it is expected C_2H_2 can play an important role in various sub-processes of soot formation and thus is a very important small species for soot prediction. Owing to the uncertainties in the fundamental chemistry, the predictions of C_2H_2 from the nine mechanisms show significant differences, which leads to differences in A1 formation pathways demonstrated by the element flux analysis of the C atom. This further indicates the importance of the fundamental chemistry in the development of aromatic chemistry and subsequent prediction of soot formation.

It is noted that the pathway flux analysis for C5 rings (i.e., C_5H_6) is also performed (see Supplement C), in which substantial differences in C_5H_6 formation pathways are observed as well. It is found that for the ABF, Naples, Aachen, Stanford, Caltech, and SJTU mechanisms, C_5H_6 is mainly produced from A1 via the following pathways: A1$\rightarrow$ A1O (C_6H_5O) $\rightarrow$ C_5H_6. Therefore, the differences in C_5H_6 formation pathways can be largely attributed to the differences in the formation pathways of A1.

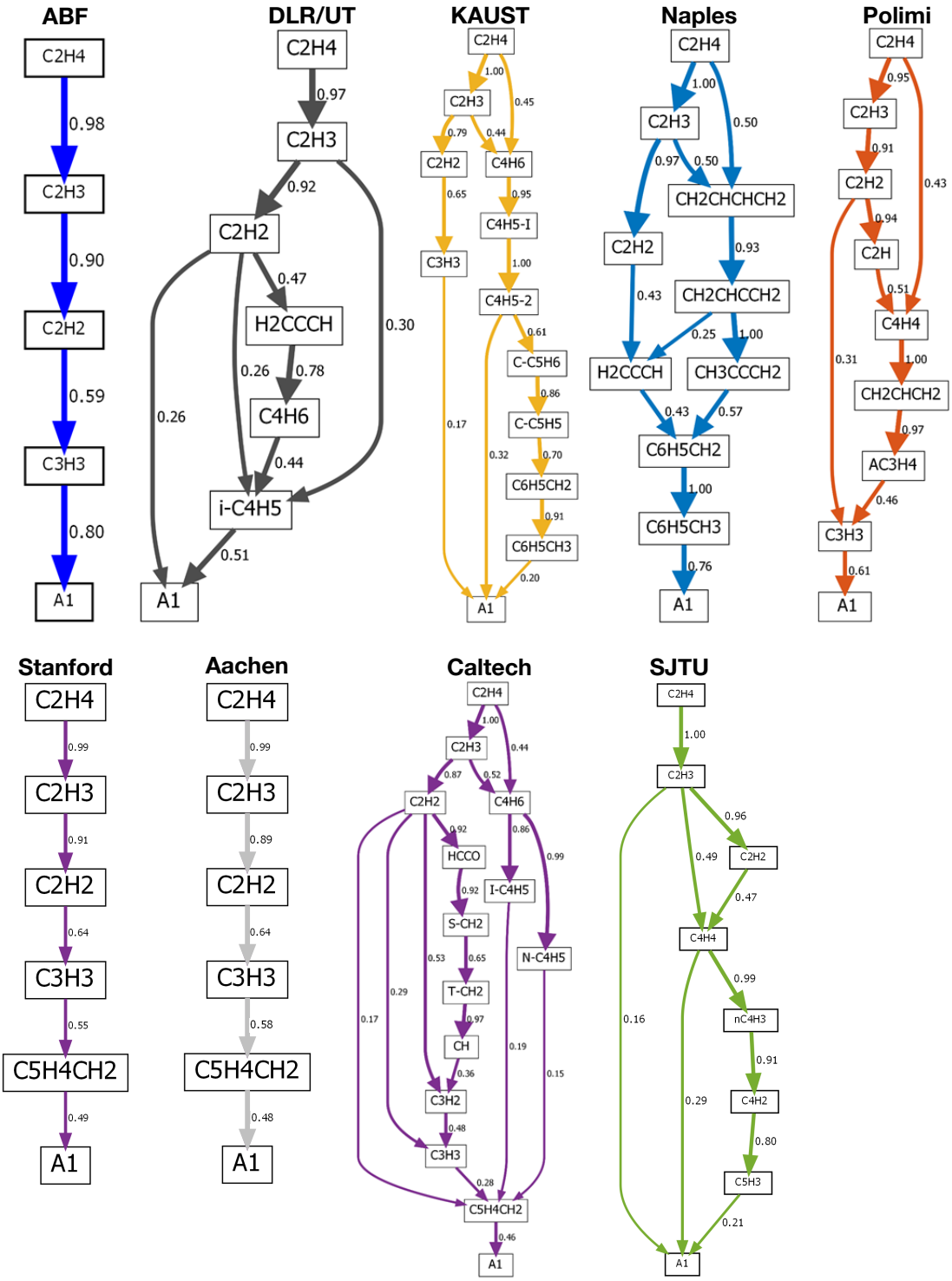

Figure 10: Reaction pathways to A1 in soot-free C_2H_4/N_2-air counterflow diffusion flames at $P = 1$ bar, in which the pathway $A \xrightarrow{n} B$ represents the contribution of the species A to the carbon mass of the species B accounting for $n \times 100\%$. For the purpose of clarity, only the pathway with inflowing flux larger than 50% of the maximum inflowing flux of species B are retained. Starting from A1 and tracing the carbon flux along with retained pathways, it will finally end at fuel, C_2H_4, such that the main growth pathways to A1 are identified.

3.3. Soot prediction

To further investigate PAH chemical reactions of the nine mechanisms, sooting counterflow C_2H_4/air diffusion flames at $a = 37.5$/s and $a = 62.5$/s [47] are simulated. It is noted that all mechanisms are coupled with the same soot model using the same model parameters required to describe nucleation, condensation, surface growth and oxidation processes. This enables the following comparisons to focus on the impact of chemical mechanisms on soot prediction only. Figure 11 shows the comparison of computed and measured soot volume fractions (f_V). It is seen that all mechanisms predict the position of the peak f_V at approximately x=3.0 mm. Nevertheless, Fig. 11 clearly demonstrates large differences in f_V predictions among the nine mechanisms. Overall, a good agreement is obtained for DLR/UT, Polimi and KAUST, while the other mechanisms significantly under-predict f_V. The highest peak f_V predicted by DLR/UT is about 60 times larger than the lowest value predicted by ABF. The DLR/UT gives a much higher prediction on f_v because it predicts a much higher value of C_2H_2 than other mechanisms, as shown in Fig. 8. On the other hand, the predictions for the position of soot inception and the zone where soot is present also show considerable scattering. In summary, it is found that the predicted f_V is very sensitive to the choice of mechanisms and that large differences exist among the predictions from the nine mechanisms.

In order to identify the dominant sources that introduce the discrepancies in soot prediction, Fig. 12 shows the growth rates of soot volume fraction via the surface reactions and the sum of PAH-based growth (nucleation and condensation). The soot oxidation is negligible compared to other processes and thus is neglected here. From Fig. 12, it can be seen that the growth rate from surface reactions is comparable to that from PAH-based routes, although the former is limited to a narrower spatial range compared to the latter. Besides, the deviation between the growth rates predicted by the mechanisms is also significant. Therefore, the differences in predictions for the growth rates of PAH-based routes and surface reactions both contribute to the large deviation in soot predictions observed in Fig. 11.

To explain the impact of PAH chemistry on the predicted f_V, the consumed mass of PAH in the whole domain is summarized in Fig. 13 for the nine mechanisms. It is seen that PAHs

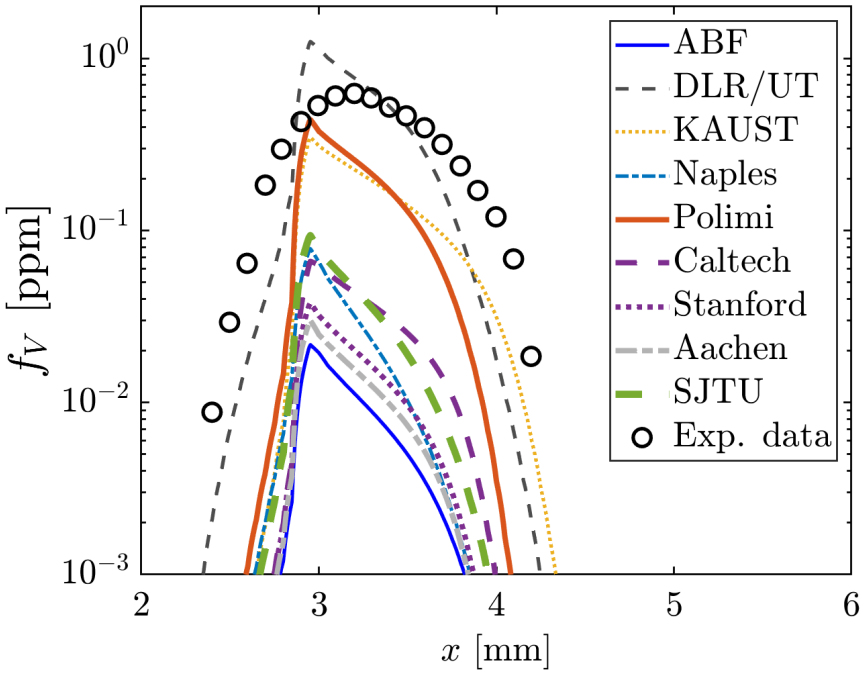

Figure 11: Comparison of computed and measured [47] soot volume fractions (f_V) in sooting C_2H_4/N_2-O_2 counterflow diffusion flame at $a = 62.5$/s and $P = 1$ atm. (For interpretation of the references to color in this figure legend, the reader is referred to the web version of this article.)

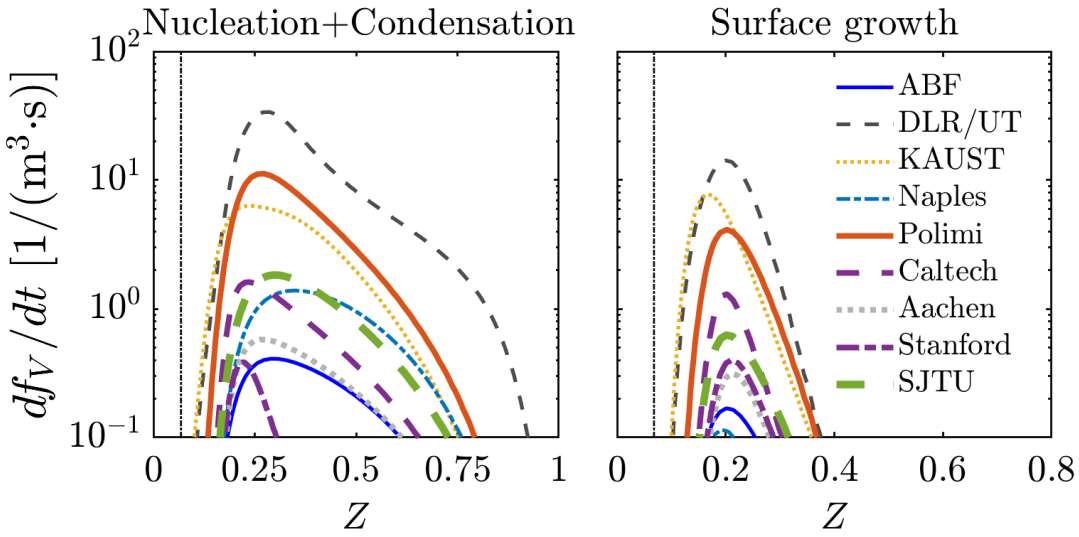

Figure 12: Soot growth rates df_v/dt from PAH-based routes (left) and surface reaction (right) in sooting C_2H_4/N_2-O_2 counterflow diffusion flame at $a = 62.5$/s and $P = 1$ atm. (For interpretation of the references to color in this figure legend, the reader is referred to the web version of this article.)

containing 2-rings (e.g. A2 and A2R5) play a dominant role in soot formation for all the mechanisms except KAUST and DLR/UT. Nevertheless, the consumption of 2-ring PAHs predicted by different mechanisms varies largely, e.g. 45 mg in Polimi vs. 7 mg in Aachen and Naples vs. 2.2 mg in ABF, leading to significantly different peak f_V in Fig. 11. Moreover, for DLR/UT and KAUST, there is a considerable conversion from PAH to soot, especially from large PAH species. This indicates that including PAHs larger than A4 promotes soot formation in DLR and KAUST. For Polimi, although only A1-A4 are included similar to ABF, Stanford, and Naples, A2 and A2R5 are formed more faster than other mechanisms (see Fig. 9), which results in a higher f_V.

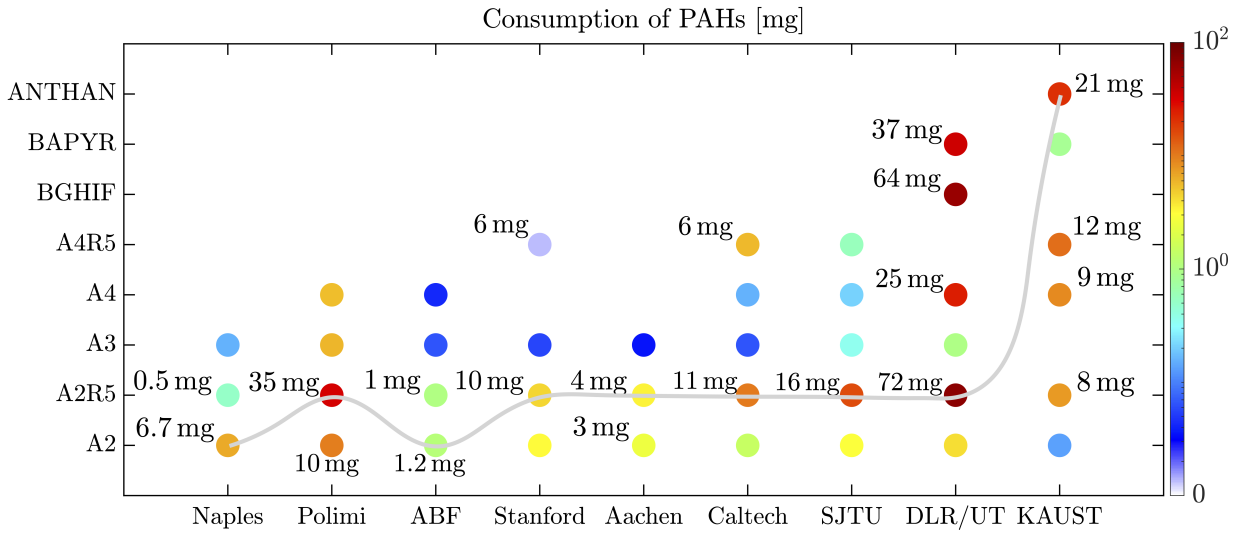

Figure 13: Consumption of PAHs per unit time in sooting C_2H_4/N_2-O_2 counterflow diffusion flame at $a = 62.5$/s and $P = 1$ atm.. The color from blue to red indicates the increase in PAH consumption. The gray line goes through the most consumed PAH in each mechanism.

Furthermore, the ability of mechanisms to capture the sensitivity of the peak f_V to strain rate is assessed. The sensitivity coefficient is defined as $d\log(f_{V,\text{peak}})/da$ [34]. Figure 14 shows the results from DLR/UT, KAUST, Caltech, SJTU, and the experiment. While Caltech and SJTU significantly under estimate f_V, they reasonably predict the sensitivity. In contrast, DLR/UT could not capture the sensitivity, while it has good performance in predicting f_V. In this sense, it cannot be easily concluded which mechanisms are better than the others, as each mechanism has its own advantages and disadvantages in predictions of f_V and its

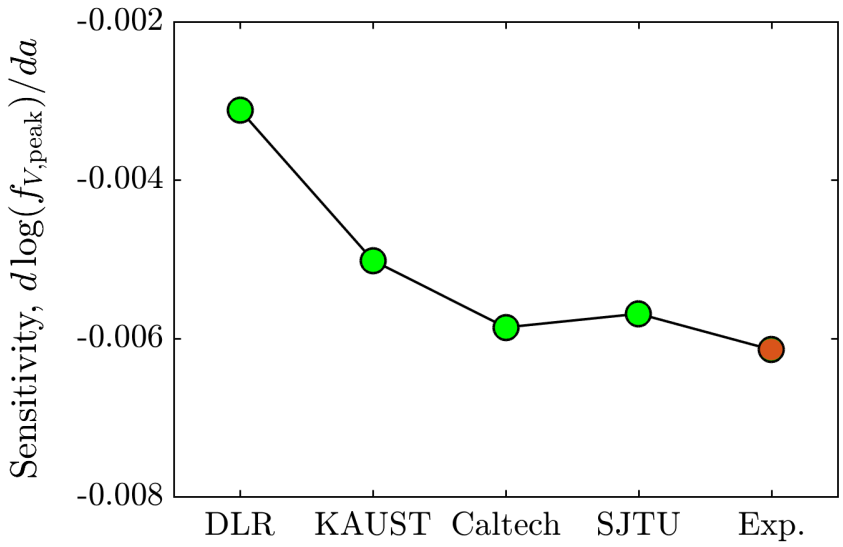

Figure 14: Comparison of computed and measured sensitivity of the peak f_V to strain rate in sooting C_2H_4/N_2-O_2 counterflow diffusion flame $P = 1$ atm. The measured data are from [47], while the computed results are from simulations based on HMOM model.

sensitivity to strain rate.

4. Conclusions

In this work, a systematic analysis of C_2H_4 mechanisms denoted as KAUST, Stanford, Aachen, Polimi, ABF, DLR/UT, Naples, Caltech, and SJTU, which have been widely used in the soot community, is performed to investigate their differences in fundamental chemistry, PAH chemistry, and soot prediction.

It is found that the nine mechanisms exhibit large differences even in predicting canonical combustion properties (e.g., ignition delay time, laminar flame speed, and extinction strain rate), indicating significant diversity in the fundamental chemistry of the nine mechanisms. The results from the sensitivity analysis show that the dominant fuel-oxidation reactions in the Naples and DLR/UT mechanisms are different from the other seven mechanisms, which makes Naples (or DLR/UT) predicting much longer IDTs (or different trends of IDT). Moreover, while the other seven mechanisms share very similar dominant fuel-oxidation reactions, their predictions for IDTs and ESRs are still rather scattered, which is attributed

to variations in the rate coefficients of sensitive reactions used in these mechanisms.

Soot precursor concentrations predicted by the nine mechanisms show large scattering. The backward element flux analysis of the C atom is conducted to explain the differences in PAH chemistry. The results indicate substantial differences in A1 formation pathways among the nine mechanisms. It is found that A1 primarily originates from the recombination of two C_3H_3 in ABF and Polimi or from an intermediate reaction where two C_3H_3 form fulvene which then isomerizes to A1 in Stanford, Aachen, and Caltech. Unlike Stanford and Aachen, the formation pathway for fulvene is augmented in Caltech through the reaction between C_2H_2 and n-C_4H_5/i-C_4H_5, which can promote A1 and PAH formation. In contrast, A1 can be directly produced via the reaction between C_2H_2 and i-C_4H_5 in DLR/UT without the involvement of fulvene. Unlike the above mentioned mechanisms, A1 is mainly formed from $C_6H_5CH_3$ through the H atom addition reaction in Naples. For KAUST, multiple pathways for A1 formation are observed, in which C_3H_3, C_4H_5-2 and $C_6H_5CH_3$ contribute equally to A1 formation. For SJTU, A1 dominantly originates from C_4H_4, C_5H_3 and C_2H_3, which is fundamentally different from the above identified pathways. The element flux analysis clearly shows the importance of small species C_2H_2 for A1 formation. Owing to the uncertainties in the fundamental chemistry, the predictions of C_2H_2 from the nine mechanisms show significant differences, which leads to the differences in A1 formation pathways demonstrated by the element flux analysis of the C atom. This further indicates the importance of the fundamental chemistry in the development of aromatic chemistry and subsequent prediction of soot formation.

Furthermore, it is found that PAHs containing two rings play a dominant role in soot formation for all the mechanisms except KAUST and DLR/UT. Nevertheless, the consumption of two-ring PAHs predicted by different mechanisms varies largely, leading to significantly different soot volume fractions. Compared to the other seven mechanisms, DLR/UT and KAUST predict higher soot volume fractions due to notable contributions of PAHs larger than A4. Moreover, it is found that while Caltech and SJTU significantly under estimate f_V, they reasonably predict the sensitivity of soot formation to strain rate. In contrast, while DLR has good performance in predicting f_V, it could not capture its sensitivity to

strain rate. In this sense, it cannot be easily concluded which mechanisms are better than the others in terms of soot prediction.

The above conclusions demonstrate that despite substantial advances in the development of C_2H_4 oxidation and PAH formation chemistry, the existing mechanisms still exhibit considerable differences in both fundamental and PAH chemistry, leading to significant variations in soot predictions when using the different mechanisms. These results suggest that the fundamental chemistry should be calibrated or improved before further development of PAH chemistry and soot models.

In summary, the present study provides the following contributions to the field of ethylene reaction mechanism and soot modeling:

- This study performs a comprehensive and systematic analysis of chemical mechanisms for ethylene oxidation, PAH formation, and soot prediction. The fundamental chemistry and PAH chemistry in the nine chemical mechanisms are assessed respectively. The results have demonstrated that there are great uncertainties in the fundamental chemistry of different chemical mechanisms.

- The dominant fuel oxidation reactions in these mechanisms are identified, and the diverse values of reaction rate coefficients used in these mechanisms are observed. Therefore, the difference in the reaction rate coefficients of dominant fuel-oxidation reactions (R1: $H+O_2=O+OH$, R2: $C_2H_3+O_2=CH_2CHO+O$, R3: $C_2H_5+O_2=C_2H_4+HO_2$, R4: $C_2H_3+O_2=CH_2O+HCO$, R5: $C_2H_4+O=CH_3+HCO$, and R6: $C_2H_4+H(+M)=C_2H_5(+M)$) could be the source of uncertainties in the fundamental chemistry. This suggest that the fundamental chemistry should be calibrated or improved before further development of PAH chemistry and soot models. This calls for the input from the researchers who have expertise on the development of chemical kinetics.

- Various analysis methods have been adopted in the present study, and a novel element backward flux analysis is conducted to identify the pathway from fuel to benzene. The present study could serve as a reference when conducting such systematic analysis of chemical mechanisms for other fuels.

It is noted that the analysis of chemical mechanisms for fuel oxidation and PAH formation is investigated in this work only for ethylene/air mixtures at a normal temperature and pressure condition. It would be of great interest to explore the differences of the nine chemical mechanisms in more complex hydrocarbon fuel/air mixtures and to examine the nine mechanisms under high temperature and pressure conditions, which will be the focus of future work.

Acknowledgments

This work was supported by National Key Research and Development Program of China (2022YFF0504500) and National Natural Science Foundation of China (No. 52176096). The authors thank Dr. Wenhao Yuan and Yuwei Deng from Prof. Fei Qi group at Shanghai Jiao Tong University for helpful discussions on the SJTU mechanism. The computational resources provided by the EPSRC/ARCHER2 through a resource allocation panel award (e679) are acknowledged.

References

[1] Y. Wang, S. H. Chung, Soot formation in laminar counterflow flames, Prog. Energy Combust. Sci. 74 (2019) 152–238.

[2] J. W. Martin, M. Salamanca, M. Kraft, Soot inception: Carbonaceous nanoparticle formation in flames, Prog. Energy Combust. Sci. 88 (2022) 100956.

[3] H. Richter, J. Howard, Formation of polycyclic aromatic hydrocarbons and their growth to soot-a review of chemical reaction pathways, Prog. Energy Combust. Sci. 26 (2000) 565–608.

[4] H. Bockhorn, A. D'Anna, A.F. Sarofim, H. Wang, Combustion generated fine carbonaceous particles, KIT Scientific Publishing, 2009.

[5] H. Wang, Formation of nascent soot and other condensed-phase materials in flames, Proc. Combust. Inst. 33 (2011) 41–67.

[6] N. Hansen, B. Yang, M. Braun-Unkhoff, A. Ramirez, G. Kukkadapu, Molecular-growth pathways in premixed flames of benzene and toluene doped with propyne, Combust. Flame 243 (2022) 112075.

[7] V. Raman, R.O. Fox, Modeling of fine-particle formation in turbulent flames, Annu. Rev. Fluid Mech. 48 (2016) 159–190.

[8] A. Raj, I. D. C. Prada, A. A. Amer, S. H. Chung, A reaction mechanism for gasoline surrogate fuels for large polycyclic aromatic hydrocarbons, Combust. Flame 159 (2012) 500–515.

[9] P. Selvaraj, P. G. Arias, B. J. Lee, H. G. Im, Y. Wang, Y. Gao, S. Park, S. M. Sarathy, T. Lu, S. H. Chung, A computational study of ethylene–air sooting flames: Effects of large polycyclic aromatic hydrocarbons, Combust. Flame 163 (2016) 427–436.

[10] H. Wang, M. Frenklach, A detailed kinetic modeling study of aromatics formation in laminar premixed acetylene and ethylene flames, Combust. Flame 110 (1997) 173–221.

[11] J. Appel, H. Bockhorn, M. Frenklach, Kinetic modeling of soot formation with detailed chemistry and physics: laminar premixed flames of C_2 hydrocarbons, Combust. Flame 121 (2000) 122–136.

[12] N. Slavinskaya, P. Frank, A modelling study of aromatic soot precursors formation in laminar methane and ethene flames, Combust. Flame 156 (2009) 1705–1722.

[13] S. B. Dworkin, Q. Zhang, M. J. Thomson, N. A. Slavinskaya, U. Riedel, Application of an enhanced pah growth model to soot formation in a laminar coflow ethylene/air diffusion flame, Combust. Flame 158 (2011) 1682–1695.

[14] N. A. Slavinskaya, U. Riedel, S. B. Dworkin, M. J. Thomson, Detailed numerical modeling of pah formation and growth in non-premixed ethylene and ethane flames, Combust. Flame 159 (2012) 979–995.

[15] V. Chernov, M. J. Thomson, S. B. Dworkin, N. A. Slavinskaya, U. Riedel, Soot formation with C1 and C2 fuels using an improved chemical mechanism for pah growth, Combust. Flame 161 (2014) 592–601.

[16] N. Slavinskaya, A. Mirzayeva, R. Whitside, J. Starke, M. Abbasi, M. Auyelkhankyzy, V. Chernov, A modelling study of acetylene oxidation and pyrolysis, Combust. Flame 210 (2019) 25–42.

[17] A. D'Anna, M. Sirignano, J. Kent, A model of particle nucleation in premixed ethylene flames, Combust. Flame 157 (2010) 2106–2115.

[18] M. Sirignano, J. Kent, A. D'Anna, Detailed modeling of size distribution functions and hydrogen content in combustion-formed particles, Combust. Flame 157 (2010) 1211–1219.

[19] G. Blanquart, P. Pepiot-Desjardins, H. Pitsch, Chemical mechanism for high temperature combustion of engine relevant fuels with emphasis on soot precursors, Combust. Flame 156 (2009) 588–607.

[20] K. Narayanaswamy, G. Blanquart, H. Pitsch, A consistent chemical mechanism for oxidation of substituted aromatic species, Combust. Flame 157 (2010) 1879–1898.

[21] G. Blanquart, Effects of spin contamination on estimating bond dissociation energies of polycyclic aromatic hydrocarbons, Int. J. Quantum Chem. 115 (2015) 796–801.

[22] L. Cai, H. Pitsch, Optimized chemical mechanism for combustion of gasoline surrogate fuels, Combust. Flame 162 (2015) 1623–1637.

[23] E. Ranzi, A. Frassoldati, R. Grana, A. Cuoci, T. Faravelli, A. Kelley, C. Law, Hierarchical and

comparative kinetic modeling of laminar flame speeds of hydrocarbon and oxygenated fuels, Prog. Energy Combust. Sci. 38 (2012) 468–501.

[24] S. Salenbauch, A. Cuoci, A. Frassoldati, C. Saggese, T. Faravelli, C. Hasse, Modeling soot formation in premixed flames using an extended conditional quadrature method of moments, Combust. Flame 162 (2015) 2529–2543.

[25] W. Yuan, Y. Li, P. Dagaut, J. Yang, F. Qi, Investigation on the pyrolysis and oxidation of toluene over a wide range conditions. i. flow reactor pyrolysis and jet stirred reactor oxidation, Combust. Flame 162 (2015) 3–21.

[26] W. Yuan, Y. Li, P. Dagaut, J. Yang, F. Qi, Investigation on the pyrolysis and oxidation of toluene over a wide range conditions. ii. a comprehensive kinetic modeling study, Combust. Flame 162 (2015) 22–40.

[27] W. Yuan, L. Zhao, S. Gaïl, J. Yang, Y. Li, F. Qi, P. Dagaut, Exploring pyrolysis and oxidation chemistry of o-xylene at various pressures with special concerns on pah formation, Combust. Flame 228 (2021) 351–363.

[28] S. Ma, X. Zhang, A. Dmitriev, A. Shmakov, O. Korobeinichev, B. Mei, Y. Li, D. Knyazkov, Revisit laminar premixed ethylene flames at elevated pressures: A mass spectrometric and laminar flame propagation study, Combust. Flame 230 (2021) 111422.

[29] W. K. Metcalfe, S. M. Burke, S. S. Ahmed, H. J. Curran, A hierarchical and comparative kinetic modeling study of C1-C2 hydrocarbon and oxygenated fuels, Int. J. Chem. Kinet. 45 (2013) 638–675.

[30] M. M. Kopp, N. S. Donato, E. L. Petersen, W. K. Metcalfe, S. M. Burke, H. J. Curran, Oxidation of ethylene–air mixtures at elevated pressures, Part 1: Experimental results, J. Propuls. Power 30 (2014) 790–798.

[31] Y. Wang, A. Raj, S. H. Chung, A PAH growth mechanism and synergistic effect on PAH formation in counterflow diffusion flames, Combust. Flame 160 (2013) 1667–1676.

[32] S. T. Chong, V. Raman, M. E. Mueller, P. Selvaraj, H. G. Im, Effect of soot model, moment method, and chemical kinetics on soot formation in a model aircraft combustor, Proc. Combust. Inst. 37 (2019) 1065–1074.

[33] A. Abdelgadir, I. A. Rakha, S. A. Steinmetz, A. Attili, F. Bisetti, W. L. Roberts, Effects of hydrodynamics and mixing on soot formation and growth in laminar coflow diffusion flames at elevated pressures, Combust. Flame 181 (2017) 39–53.

[34] S. Kruse, A. Wick, P. Medwell, A. Attili, J. Beeckmann, H. Pitsch, Experimental and numerical study of soot formation in counterflow diffusion flames of gasoline surrogate components, Combust. Flame 210 (2019) 159–171.

[35] D. Zhou, S. Yang, Soot-based global pathway analysis: Soot formation and evolution at elevated

pressures in co-flow diffusion flames, Combust. Flame 227 (2021) 255–270.

[36] P. Liu, J. Guo, E. Quadarella, A. Bennett, S. R. Gubba, S. Saxena, O. Chatakonda, J. W. Kloosterman, X. He, H. G. Im, W. L. Roberts, The effect of preheating temperature on pah/soot formation in methane/air co-flow flames at elevated pressure, Fuel (2021) 122656.

[37] C. Bowman, R. Hanson, D. Davidson, J. W.C. Gardiner, V. Lissianski, G. Smith, D. Golden, M. Frenklach, M. Goldenberg, GRI-1.2, http://www.me.berkeley.edu/gri-mech (1995).

[38] K. J. Hughes, T. Turányi, A. R. Clague, M. J. Pilling, Development and testing of a comprehensive chemical mechanism for the oxidation of methane, Int. J. Chem. Kinet. 33 (2001) 513–538.

[39] G. P. Smith, D. M. Golden, M. Frenklach, N. W. Moriarty, B. Eiteneer, M. Goldenberg, C. T. Bowman, R. K. Hanson, S. Song, J. William C. Gardiner, V. V. Lissianski, Z. Qin, GRI-3.0, http://www.me.berkeley.edu/gri-mech (1998).

[40] B. Eiteneer, M. Frenklach, Experimental and modeling study of shock-tube oxidation of acetylene, Int. J. Chem. Kinet. 35 (2003) 391–414.

[41] S. G. Davis, A. V. Joshi, H. Wang, F. Egolfopoulos, An optimized kinetic model of H2/CO combustion, Proc. Combust. Inst. 30 (2005) 1283–1292.

[42] Caltech mechanism, 2015. URL: `https://www.theforce.caltech.edu//CaltechMech/index.html`.

[43] S. Dong, S. W. Wagnon, L. Pratali Maffei, G. Kukkadapu, A. Nobili, Q. Mao, M. Pelucchi, L. Cai, K. Zhang, M. Raju, T. Chatterjee, W. J. Pitz, T. Faravelli, H. Pitsch, P. K. Senecal, H. J. Curran, A new detailed kinetic model for surrogate fuels: C3mechv3.3, Applications in Energy and Combustion Science 9 (2022) 100043.

[44] D. G. Goodwin, H. K. Moffat, R. L. Speth, Cantera: An object-oriented software toolkit for chemical kinetics, thermodynamics, and transport processes. version 2.2.0 (2015).

[45] J. Huo, T. Shu, Z. Ren, C. K. Law, Extrapolation of laminar ethylene/air flame speeds at elevated pressures with flame chemistry analysis, J. Propuls. Power 35 (2018) 424–431.

[46] L. Figura, A. Gomez, Structure of incipiently sooting ethylene–nitrogen counterflow diffusion flames at high pressures, Combust. Flame 161 (2014) 1587–1603.

[47] Y. Wang, S. H. Chung, Strain rate effect on sooting characteristics in laminar counterflow diffusion flames, Combust. Flame 165 (2016) 433–444.

[48] T. Zirwes, F. Zhang, P. Habisreuther, M. Hansinger, H. Bockhorn, M. Pfitzner, D. Trimis, Quasi-DNS dataset of a piloted flame with inhomogeneous inlet conditions, Flow Turbulence Combust. 104 (2020) 997–1027.

[49] M. E. Mueller, G. Blanquart, H. Pitsch, Hybrid Method of Moments for modeling soot formation and growth, Combust. Flame 156 (2009) 1143–1155.

[50] M. E. Mueller, H. Pitsch, Les model for sooting turbulent nonpremixed flames, Combust. Flame 159

(2012) 2166–2180.

[51] A. Attili, F. Bisetti, M. E. Mueller, H. Pitsch, Formation, growth, and transport of soot in a three-dimensional turbulent non-premixed jet flame, Combust. Flame 161 (2014) 1849–1865.

[52] A. Attili, F. Bisetti, M. E. Mueller, H. Pitsch, Damköhler number effects on soot formation and growth in turbulent nonpremixed flames, Proc. Combust. Inst. 35 (2015) 1215–1223.

[53] A. Attili, F. Bisetti, M. E. Mueller, H. Pitsch, Effects of non-unity lewis number of gas-phase species in turbulent nonpremixed sooting flames, Combust. Flame 166 (2016) 192–202.

[54] S. Deng, M. E. Mueller, Q. N. Chan, N. H. Qamar, B. B. Dally, Z. T. Alwahabi, G. J. Nathan, Hydrodynamic and chemical effects of hydrogen addition on soot evolution in turbulent nonpremixed bluff body ethylene flames, Proc. Combust. Inst. 36 (2017) 807–814.

[55] W. Han, V. Raman, M. E. Mueller, Z. Chen, Effects of combustion models on soot formation and evolution in turbulent nonpremixed flames, Proc. Combust. Inst. 37 (2019) 985–992.

[56] Y. Wang, W. Han, A. Attili, Z. Chen, Numerical analysis of very rich propagating spherical flames: Soot formation and its impact on the determination of laminar flame speed, Combust. Flame 237 (2022) 111860.

[57] J. Revel, J. Boettner, M. Cathonnet, J. Bachman, Derivation of a global chemical mechanism for methane ignition and combustion, J. Chim. Phys. 91 (1994) 365–382.

[58] C. K. Law, Combustion Physics, Cambridge University Press, 2006.